Radiograph Manufacturer and Model Identification Using Deep-RSI

Farid Ghareh Mohammadi[1,2] and Ronnie Sebro[1,2]
[1]Department of Radiology, Mayo Clinic, Jacksonville, Fl, USA
[2]Center for Augmented Intelligence, Mayo Clinic, Jacksonville, Fl, USA

Gharehmohammadi.farid@mayo.edu
Sebro.ronnie@mayo.edu

Abstract: Malware attacks of healthcare institutions are simultaneously becoming more common and more sophisticated. Artificial intelligence (AI) has resulted in the ability to rapidly alter or generate false images, advancing the ease of forgery of digital images. Digital image manipulation and substitution of radiographs are major threats to healthcare institutions because these altered images may affect patient care. Identifying the source (manufacturer, model) of radiology images is one method of validating the origin of radiology images in a healthcare system. In a previous study, researchers demonstrated that features from magnetic resonance imaging (MRI) could be used to trace and authenticate the source of the MRI images. We previously developed and tested the Deep learning for Radiograph Source Identification (Deep-RSI) approach for source identification of radiographs obtained of the upper extremities (hands, wrists, forearms, elbows, and shoulders). In this research, we present an empirical and quantitative investigation using deep learning to validate the source of digital radiographic images of the lower extremities (knees, legs, ankles, and feet). A convolutional neural network (CNN) is employed to extract features, which are then followed by three fully connected layers (FCNN). To ensure that our proposed method is a content-free approach, we added a new layer before the CNN to extract the initial content-free pixels and train the features using the CNN and FCNN layers. This proposed approach was used to identify the source of each digital image of a lower extremity. Adult patients of both sexes who had radiographs of the lower extremities at Mayo Clinic between 01/01/2010 and 12/31/2021 were evaluated. The data was randomly split by patient into training/validation and test datasets. There were 9 radiographic machine models and 6 manufacturers. Deep-RSI had an accuracy of 99.00% (AUC= 0.99) and 97.00% (AUC=0.94) for detecting the manufacturer and model of the radiographic machine for radiographs of the feet respectively, confirming that forensic evaluation of radiographs can be performed. This is the first medical forensics examination of this type to identify and confirm the source origins for radiographs of the lower extremities. This technique may be helpful to detect radiology malware attacks and scientific fraud.

Key words: Deep Learning, Medical Forensics, Lower Extremities, Radiology, Source Identifications

1. Introduction

The main purpose of forgery of an image is to hide or alter details in the images so that the images can be used to falsely convey different information (Jaiswal & Srivastava, 2022). Artificial Intelligence (AI) is currently used in digital image manipulation, which has become a major issue in a variety of industries, including social media, medical imaging, digital forensics and scientific publications. As AI technology advances it is more difficult for a professional to discern a real from fake image. This increases of the likelihood of a successful digital image forgery. Digital image manipulation and computer-generated fake radiographs are extreme threats to healthcare institutions because these altered radiographs may adversely affect patient care. This will have a negative impact on patients and respected institutions.

Generative Adversarial Networks (GANs) (Goodfellow et al, 2020) are a type of generative deep learning model that generate computer-generated fake images and text data (Deepfakes). Hackers use these advanced tools to increase the likelihood of seamless forging of digital images. Deepfakes have arisen as a severe threat to the security of healthcare institutions and is a significant threat particularly in radiology because fake digital radiographs are difficult to detect. Currently radiologists interpret radiographs without confirming of the source of the images or verifying that the radiographs are not fakes. However, if these radiographs are altered or manipulated, radiologists may be unable to detect real from fake radiographs. Altering or replacing radiographs poses serious risks to healthcare institutions because these radiographs are used for diagnosis. This can delay patient care and affect patient prognosis. Validating the radiographs through detecting the source (manufacturer and model) of the radiographs is an important step in finding the solution to this important issue. There are a few proposed solutions employing AI to detect this forgery in medical images which are limited to (Fang et al, 2020), (Ghareh Mohammadi & Sebro, 2022), so we propose expanding this fraud detection methodology using a different dataset (radiographs of the lower extremities) by utilizing the source identification solution. In this paper, we propose to leverage AI to predict the radiographs sources (manufacturer and model of radiographic machine) to detect forgery of digital radiographs.

2. Materials and Methods

The study protocol was reviewed and approved by the Mayo Clinic Institutional Review Board (IRB). Data collection was in accordance with the Health Insurance Portability and Accountability Act (HIPAA). We followed the ethical principles for medical research involving human subjects, including research on identifiable human material and data according to Declaration of Helsinki.

Patients

The study patients were individuals who had radiographs of the knees, legs, ankles, and feet at Mayo Clinic between 01/01/2010 and 12/31/2021. We randomly split the patients into train/validation (n=80%) and test(n=20%) datasets, so that the dataset partitions are independent.

Radiographic machines

Radiographs were taken using General Electric (GE) healthcare (General Electric, Waukesha WI), Canon (Tustin, CA), Carestream Health (Rochester, NY), Philips Medical Systems (Amsterdam, Netherlands), and Siemens Healthineers (Erlangen, Germany) manufacturers. We excluded manufacturers and models if there were less than 50 patients per each class of both manufacturer and model. We converted radiographic machine manufacturer' and model's names into unique numbers for confidentiality.

Radiographic technique

Radiographs of the knees were taken in one or more of the anterior-posterior (AP), posterior-anterior (PA) flexed, patellar, internal oblique, external oblique, and lateral projections. Ankle radiographs were taken in the AP, lateral, or mortise projections; while leg radiographs were taken in the AP and lateral projections. Foot radiographs were taken in the AP, lateral, and oblique projections. The radiographs originate from different sites (knees, legs, ankles, and feet) and were obtained in different projections with varying angles, so it is difficult to match the contents of images to the origin of the radiographic machines. Most patients had at least three images as part of their radiology study.

Image pre-processing

Radiographs were downloaded from the Visage Picture Archiving and Communications System (PACS) in Digital Imaging and Communications in Medicine (DICOM) format. These images were then converted to the Joint Photographs Expert Group (JPEG) format and resized to 256x256. The image pixel intensities were normalized to the range 0 to 255. We generate a batch of images by adding relevant weights to each instance during training process to deal with class imbalance between manufacturers and models. The weights are proportional to the frequency of the unique labels in the dataset. We apply the weights when we select instances for batches. At the end, we have a batch of data with a suitable number of images per class in every batch.

Experiment:

We used the deep learning model to predict the (1) radiographic machine manufacturer and (2) the radiographic machine model. We used the following deep learning architecture for both experiments.

Architecture

We use deep learning for radiographs source identification (Deep-RSI) to extract features on-line to generate a model on the train dataset in order to predict the radiographic machine source (manufacturer and model) in the test dataset. Figure 1 shows the order of the process: input, deep learning and output.

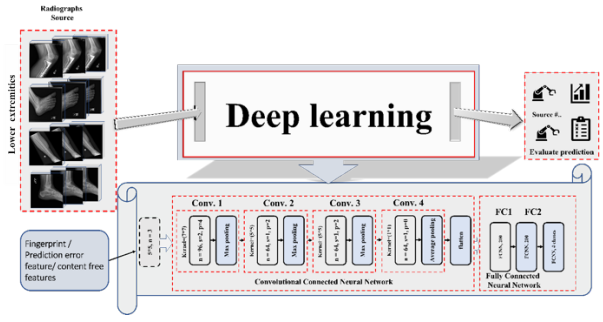

Figure 1: Content-free deep learning architecture for radiographs manufacturer and model Identification

Fingerprint feature extraction

Normally, digital images intensities are derived from three channels: red, green, and blue (RGB). The deep learning algorithm uses all the image content pixels' value which are called image intensities. These pixel intensities serve as inputs to the deep learning model. We convert gray-scale radiographs to single-channel images. We add a layer at the beginning of CNN layers to extract low-level features from content-free pixels using a kernel filter with a size of (5*5) (Figure 1). This layer uses 3 filters of the same size to perform like three-channel images which is also referred to as fingerprint, residual images, prediction error feature / content free features. This layer keeps only pixels (noise) that are sparsely distributed in the images. Majority of pixels in the images are black (i.e., the intensity values are close to zero). The extracted information from the content-free pixels is used as the input for the subsequent analyses. We use the CNN to extract 6272 high-level features from the low-level features.

CNN

We use four convolutional layers within the CNN. The first layer uses 96 filters with a filter (kernel) size of (7*7) and operates on stride=2 while taking padding (p =4) into account (Figure 1). Padding (p=1) is a zero-value pixel added to the periphery of the input image. When p is equal to four, it means that we add four pixels with normalized intensity of 0 to the periphery of the input image. Pixels at the edge of the images can be erroneously ignored during the feature extraction. Padding helps the CNN feature extractor to evaluate all pixels, including pixels located at the border/edge of images.

We compute all the filters to generate the initial high-level features in the first layer. We apply a max-pooling function with a configuration of (size = (2*2) and stride =2) to shrink the dimension of generated high-level features within each channel by half while keeping the number of channels (96).

The second layer uses the output of the first layer (96 channels) to apply 64 filters with stride =1, after applying padding(p=2). We use a filter size of (5*5) to generate 64 channels with the same input size. We apply the max-pooling with size = (2*2) and stride=2 to reduce the dimension of each channel by half.

In the third layer, we repeat the identical configuration of the second layer (the same filter count and size, stride=1 and padding=2). We also apply the max-pooling function with size = (2*2) and stride =2 to decrease the dimension of each channel by half in this layer as well.

In the final layer, we utilize 64 filters with a size of (1*1) with stride =1 and padding(p=0), which means that we do not add padding in this layer. We apply an average-pooling with size = (2*2) and stride = 2. Finally, we flatten the output of the fourth layer to prepare it for training process by FCNN.

FCNN

We leverage the FCNN as our main classifier with three layers (Figure 1). The first FCNN layer computes 6272 features using 200 nodes to generate weights and uses a rectified linear unit (ReLU) which is an activation function to filter input wights. If the input is positive, ReLU outputs it directly; otherwise, it outputs zero. The layer passes filtered weights to the second layer with 200 nodes with ReLU. The third layer employs a softmax function coupled with a value equal to the number of classes to build a probility of predicting output class. FCNN selects the class prediction with the greatest probability.

Software

We conduct this research in Python=3.10.8 using deep learning libraries: Pytorch=1.13.1, Pytorch-cuda=11.7 and Torch=1.13.1. We evaluate the hyper-parameters with different values to obtain the optimal validation learning rate values with 0.1, 0.01, 0.001, 0.0001. We choose the Adam optimizer and set a learning rate equal to 0.0001, epochs equal to 50, and batch size equal to 20.

Hardware

We run this research study on a system with the following configurations: GPU: NVIDA Quadro RTX 4000 (DRAM: 8GB), CPU: Intel® Xeon® W-2123, 3.60 GHz, and random-access memory (RAM):64 GB.

Model performance statistics

In this research, we use five key metrics to evaluate the Deep-RSI classification performance in both experiments: manufacturer identification and model identification. Statistics were calculated using the scikit-learn Python library.

1) Accuracy: This metric measures the overall performance of classification performance independent of classes using formula 1.

$$\text{Accuracy} = \frac{TP+TN}{P+N} \quad \text{(Formula 1)}$$

Where TP stands for true positive, TN is true negative, P stands for the number of positive samples and N stands for the number of negative samples.

2) Area under curve (AUC): We use this measure to calculate the ratio of false positive rate (FPR) against true positive rate (TPR). AUC also measures the whole area underneath the entire receiver operating characteristic (ROC) curve from (0,0) to (1,1) using formula 2. ROC plots a chart using the FPR (on x axis) and TPR (on y axis). FPR is the ratio of false positive over the sum of false positive and true negative.

$$\text{AUC} = \int_0^1 ROC \, dx \quad \text{(Formula 2)}$$

3) Specificity: This measure is also known as the true negative rate (TNR) where we look for negative samples which are correctly classified using formula 3.

$$\text{Specificity} = \frac{TN}{TN+FP} = \frac{TN}{N} \quad \text{(Formula 3)}$$

4) Sensitivity: This is the true positive rate (TPR) in which we measure the rate of correctly classified positive samples according to formula 4. Sensitivity is also known as recall.

$$\text{Recall} = \text{Sensitivity} = \frac{TP}{TP+FN} = \frac{TP}{P} \quad \text{(Formula 4)}$$

where FN is the number of positive samples incorrectly predicted negatives, and P is the number of positive samples.

5) Positive Predictive value (PPV) or Precision: This measurement is the ratio of the true positives to the number of true positives and false positives.

$$\text{PPV} = \text{Precision} = \frac{TP}{TP+FP} \quad \text{(Formula 5)}$$

6) Negative Predictive Value (NPV): NPV is the ratio of the number of true negatives to the sum of the true negatives and false negatives

$$\text{NPV} = \frac{TN}{TN+FN} \quad \text{(Formula 6)}$$

3. Results

Experiment 1

In experiment 1, we assessed the proposed method on radiographs manufacture classification for each site (Table 1).

Table 1: Experiment 1: Radiographic machine manufacturer classification for radiographs of the lower extremities

Site	Total Patients	Total Images	Train/ Validation (patients)	Train/ Validation (images)	Test (patients)	Test (images)	No of classes (test)	Weighted average Accuracy (images)	Weighted average AUC (images)
Knees	1418	6119	1132	4849	286	1270	4	0.96	0.95
Legs	616	2177	494	1726	122	451	3	0.95	0.93
Ankles	1290	4598	1038	3692	252	906	5	0.97	0.95
Feet	1074	3986	859	3183	215	803	3	0.99	0.99

Table 2: Experiment 1: Detecting the radiographic machine manufacturer for radiographs of the knees, legs, ankles and feet

Body site							
Knees							
Manufacturer	No. of samples	Accuracy	AUC	Specificity	Sensitivity	PPV	NPV
Class 0	237	0.97	0.93	0.99	0.88	0.94	0.97
Class 1	202	0.99	0.98	0.99	0.96	0.95	0.99
Class 2	45	0.99	0.93	0.99	0.87	0.95	0.99
Class 3	786	0.96	0.96	0.93	0.98	0.96	0.97
Legs							
Class 4	332	0.96	0.95	0.95	0.96	0.98	0.90
Class 5	48	0.94	0.86	0.97	0.75	0.73	0.97
Class 6	71	0.92	0.87	0.95	0.80	0.74	0.96
Ankles							
Class 7	25	0.99	0.99	0.99	1.0	0.78	1.0
Class 8	74	0.99	0.95	1.0	0.90	1.0	0.99
Class 9	82	0.97	0.96	0.98	0.94	0.80	0.99
Class 10	208	0.96	0.94	0.98	0.89	0.92	0.97
Class 11	517	0.99	0.99	0.99	0.98	0.99	0.98
Feet							
Class 12	199	0.99	0.99	0.99	0.98	0.98	0.99
Class 13	211	0.99	0.99	0.99	0.99	0.97	0.99
Class 14	393	0.99	0.99	0.99	0.98	0.99	0.98

Knee radiograph manufacturer analysis: Table 2 shows the results of knee radiographs' analysis for the four imbalanced classes. The proposed method obtained the highest *accuracy* with values of 0.99 and 0.99 for *class 1* and *class 2*, respectively. *Class 1* is the most easily identified manufacturer for classification of the radiographic machine used to obtain knee radiographs. The proposed method obtained the highest *AUC* for class 1 (AUC=0.98).

Leg radiograph manufacturer analysis: Class 4 is the most easily identified manufacturer for radiographs of the legs and our model had *accuracy, AUC, sensitivity* and *PPV* of 0.96, 0.95, 0.95, 0.96 and 0.98, respectively to detect radiographs created by Class 4.

Ankle radiograph manufacturer analysis: Ankles radiographs were all taken using 1 of 5 radiographic machine manufacturers. The proposed method had a high accuracy of 0.99 and AUC > 0.94 for identifying which radiographic machine was used to obtain ankle radiographs.

Foot radiograph manufacturer analysis: Again, our proposed method had > 0.99 *accuracy* and *AUC* to correctly predict which radiographic machine was used to obtain a patient's foot radiographs.

Experiment 2

In this experiment, we try to identify the model of the radiographic machine used to create radiographs of the knees, legs, ankles, and feet. Each dataset has a different number of classes: Knees and feet have 5 classes, legs have 3 classes, and ankles have 4 classes. We assessed model datasets and obtained results of average classification *accuracies* and *AUCs* for determining the model used for creating the knee, leg, ankle, and foot radiographs which are shown in Table 3. Table 3 redemonstrates that we can predict the radiographic machine model used to generate leg radiographs with accuracy and AUC of 0.99 and 0.99, respectively. Despite the imbalance of our dataset, both accuracy and AUC are high. This verifies that the proposed method produces a model that is not biased toward the dominant class.

Table 3: Experiment 2: Radiographic machine model classification for radiographs of the lower extremities

Site	Total Patients	Total Images	Train/ Validation (patients)	Train/ Validation (images)	Test (patients)	Test (images)	No of classes (test)	Average Accuracy (images)	Average AUC (images)
Knees	1326	5431	1070	4579	256	852	5	0.97	0.94
Legs	546	1888	437	1518	109	370	3	0.99	0.99
Ankles	1086	3849	952	3429	134	420	4	0.98	0.98
Feet	1074	3983	957	3132	117	851	5	0.97	0.94

Classification results for radiographics machine models across four sites are shown in Table 4. The experimental findings show that the model has high accuracy and AUC to identify the radiographic machine model used to create radiographs with values of 0.99 and 0.99 respectively.

Table 4: Detecting the radiographic machine model for radiographs of the knees, legs, ankles, and feet

Body site							
Knees							
Classes	No. of images	Accuracy	AUC	Specificity	Sensitivity	PPV	NPV
Class 0	75	0.95	0.83	0.98	0.68	0.78	0.97
Class 1	144	0.98	0.96	0.99	0.93	0.98	0.98
Class 2	26	0.99	0.90	0.99	0.81	0.84	0.99
Class 3	534	0.97	0.96	0.94	0.98	0.96	0.97
Class 4	73	0.95	0.86	0.96	0.75	0.67	0.98
Legs							
Class 5	70	0.99	0.98	0.99	0.97	0.96	0.99
Class 6	43	0.98	0.94	0.99	0.88	0.93	0.98
Class 7	257	0.99	0.98	0.97	0.99	0.99	0.98
Ankles							
Class 8	42	0.98	0.97	0.98	0.95	0.85	0.99
Class 9	26	0.99	0.99	0.99	1.0	0.96	1.0
Class 10	228	0.99	0.99	1.0	0.99	1.0	0.99
Class 11	124	0.97	0.96	0.99	0.93	0.97	0.97
Feet							
Class 12	105	0.93	0.84	0.96	0.72	0.72	0.96
Class 13	36	0.97	0.86	0.98	0.75	0.63	0.99
Class 14	174	0.97	0.95	0.98	0.91	0.93	0.98
Class 15	449	0.97	0.97	0.98	0.96	0.98	0.96
Class 16	87	0.94	0.85	0.96	0.75	0.70	0.97

Our model consistently could predict the model of the radiographic machine used to obtain radiographs of the knee, leg, ankles, and feet (Table 4).

4. Conclusion

We created a deep learning model to detect the make and model of the radiographic machine used to take radiographs with high accuracy and high AUC. Our model could reliably do this using 4 different datasets, with no change in accuracy or AUC between the training/validation dataset and the test datasets. We used the content- free pixel information to detect the radiographic machine source for radiographs of the different sites

in the lower extremities. This is a novel extension of previously published method based on analysis of content-free pixel information from digital cameras, applied to digital radiographs.

Radiograph source identification has scientific, medical, and legal implications. First, scientists may be able to spot scientific fraud, such as cut-and-paste radiographs from inconsistent sources. Second, if a healthcare system is hacked and fake radiographs are placed in a patient's medical record, then the patient's diagnosis and treatment may be altered. Third, if there is a medical malpractice case and the radiograph with a critical finding to the case is replaced by a fake radiograph, then justice may not be served, and the patient may not be compensated for the medical error. We developed a deep learning-based approach to make use of content-free pixel information as the first step to detect forgery via source identification solution.

There are series of research studies in which scientists used machine learning to train a model for source identification using extracted imaging features. Initially, researchers extracted a list of features followed by using support vector machine (SVM), artificial neural network (ANN) and random forest (RF) (Zhang et al, 2020). In (You et al, 2020) researchers looked for the sources of light using statistical fluctuations and correlation properties of features followed by using ANN and naïve Bayes (NB) classifiers for training and evaluating the trained model for sake of the source identification problem. Machine learning approaches were not efficient because of the manual feature extraction process ((You et al, 2020). There was a need for automatic feature extraction and learning strategies to improve efficiency. Deep learning is an effective way to extract features automatically and train the model based on these features simultaneously. Researchers used the trained model for source classification problem to classify test datasets (Freire-Obregon et al, 2019). Deep learning is an advanced learning technology in which we use a convolutional neural network (CNN) and classifier, a fully connected neural network (FCNN). The CNN extracts various numbers of features using different convolutional layers. Every layer shares a kernel filter, with an activation function, stride, and padding. The FCNN uses the collected features to create a model with a softmax function in the last layer for source prediction. Source prediction is an important first step in image authentication.

Researchers divided the image authentication approaches into two categories: active and passive authentication (Al-Qershi & Khoo, 2013). In active authentication, the goal is to identify an actively hidden object / actively placed watermark or digital signature in the images. The images are altered to confirm the originality of images by embedding a watermark image or using a signature (Al-Qershi & Khoo, 2013). These actively placed object is known and can be detected by the forensic expert. Passive authentication is different from active authentication because there is no actively placed object embedded in the images. Passive authentication can be used to identify an image where only a region within the image is altered. Identifying these fabricated regions is also challenging and requires region-based steganalysis approaches (Ghareh Mohammadi & Sajedi, 2017). We focus on the content-free pixels which are sometimes considered noise. Researchers have shown that the noise pixels contain information content that could be used to determine the device used to create an image (Ghareh Mohammadi & Sebro, 2022). In general, all types of medical/non-medical cameras leave identifiable noise while creating images/radiographs due to different capturing process and technologies. We exploit intrinsic noise in the radiographs in such a way that we can predict the source of the radiographs.

Researchers developed several approaches for extracting information from the noise in the digital images. This noise is referred to as content-free pixel information, and these are the primary pixels essential for solving this problem. Originally, researchers extracted the noise pixel information directly from images to identify the source of images. They utilized Photo Response Non Uniformity (PRNU) (McCleary, 2009), (Rosenfeld & Sencar, 2009) and Sensor Pattern Noise (SPN) (Lukas et al, 2006) to extract relevant information from images. Peak to Correlation Energy (PCE) ratio was used to assess the extracted noise information for source identification (Goljan et al, 2009), (Kang et al, 2011). Researchers even studied whether the noise varied between photographs that were obtained by a professional or amateur to determine if the noise was intrinsic to the device or the user (Rosenfeld & Sencar, 2009).

Prior studies have shown that there is a way to relate digital images/videos to the device used to create these digital images/videos (Al-Qershi & Khoo, 2013). However, there is little known about source identification of medical images. Advanced AI techniques, particularly deep learning-based approaches, were first used for MRI source identification (Fang et al, 2020), which is the first forensic research study of this type in the medical field. Ghareh mohammadi and Sebro in (Ghareh Mohammadi & Sebro, 2022) expanded this approach for radiograph source identification. They conducted a Deep-RSI approach to identify the manufacturer and model of the upper extremities' radiographs (Ghareh Mohammadi & Sebro, 2022). In this paper, we used a modified Deep-RSI approach for source identification of lower extremities radiographs.

The main limitation in this work is that there were a limited number of manufacturers and models used to generate the radiographs. This is the typical number of devices at a large tertiary care healthcare institution. However, in future we will investigate the performance of our model with larger number of manufacturers and models. Radiographs were taken from different angles, which may have influenced the performance of the model. If we have enough radiographs from all different angles, we might have higher performance. Finally, the data all come from a single tertiary care academic center, and the devices investigated may not generalize to all radiographic machines.

In summary, we use a deep learning model to investigate lower extremity radiographs to accurately predict the make and model of the machine that generated the radiograph.

References

Al-Qershi, O. M. & Khoo, B. E. (2013) Passive detection of copy-move forgery in digital images: State-of-the-art. *Forensic science international*, 231(1-3), 284-295.

Fang, S., Sebro, R. A. & Stamm, M. C. (2020) A deep learning approach to MRI scanner manufacturer and model identification. *Electronic Imaging*, 217-1 -- 217-6.

Freire-Obregon, et al (2019) Deep learning for source camera identification on mobile devices. *Pattern Recognition Letters*, 126, 86-91.

Ghareh Mohammadi, F. & Sajedi, H. (2017) Region based image steganalysis using artificial bee colony. *Journal of Visual Communication and Image Representation*, 44, 214-226.

Ghareh Mohammadi, F. & Sebro, R. (2022) Deep-RSI: Deep learning for Radiographs Source Identification *2022 international conference on computational science and computational intelligence (csci)*, Pressing.

Goljan, M., Fridrich, J. & Filler, T. (2009) Large scale test of sensor fingerprint camera identification, *Media forensics and security*. SPIE.

Goodfellow, I., et al. (2020) Generative adversarial networks. *Communications of the ACM*, 63(11), 139-144.

Jaiswal, A. K. & Srivastava, R. (2022) Detection of copy-move forgery in digital image using multi-scale, multi-stage deep learning model. *Neural Processing Letters*, 54(1), 75-100.

Kang, X., et al. (2011) Enhancing source camera identification performance with a camera reference phase sensor pattern noise. *IEEE Transactions on Information Forensics and Security*, 7(2), 393-402.

Lukas, J., Fridrich, J. & Goljan, M. (2006) Digital camera identification from sensor pattern noise. *IEEE Transactions on Information Forensics and Security*, 1(2), 205-214.

McCleary, B. (2009) *Digital imaging system testing and design using physical sensor characteristics*University of Southern California.

Rosenfeld, K. & Sencar, H. T. (2009) A study of the robustness of PRNU-based camera identification, *Media Forensics and Security*. SPIE.

You, C., et al (2020) Identification of light sources using machine learning. *Applied Physics Reviews*, 7(2), 021404.

Zhang, H., et al (2020) Machine learning-based source identification and spatial prediction of heavy metals in soil in a rapid urbanization area, eastern China. *Journal of Cleaner Production*, 273, 122858.